*J. Phys. Chem. A* **2000,** *104,* 5141−5148

# Gas-Phase Reactions of HONO with HNO and $NH_3$: an Ab Initio MO/TST Study

**Xin Lu,[†] Ryza N. Musin, and M. C. Lin***

*Department of Chemistry, Emory University, and Cherry L. Emerson Center for Scientific Computation, Emory University, Atlanta, Georgia 30322*

*Received: February 4, 2000; In Final Form: March 20, 2000*

The reduction of HONO by HNO and $NH_3$ has been investigated by means of ab initio molecular orbital and transition-state theory (TST) calculations. The main reaction channels for the HNO + *trans*-HONO (*cis*-HONO) reactions are those proceeding via five-member ring transition states, leading to the production of NO and $H_2O$. In the temperature range 300−1000 K, TST calculations predict an A factor of $2.25 \times 10^{10}$ $cm^3$ $mol^{-1}$ $s^{-1}$ (or $3.63 \times 10^{10}$ $cm^3$ $mol^{-1}$ $s^{-1}$) and an apparent activation energy of 20.9 kcal/mol (or 21.9 kcal/mol) for the HNO + *trans*-HONO (or *cis*-HONO) reaction. In the $NH_3$ + HONO system, the reaction $NH_3$ + *cis*/*trans*-HONO → $H_2NNO$ + $H_2O$ with barrier heights centering around 34 kcal/mol can occur at high temperatures. The reversible H-atom exchange reaction $N\mathbf{H}_3$ + *cis*-HONO ⇔ $\mathbf{H}_2N\mathbf{H}$−O(H)NO ⇔ $N\mathbf{H}_2H$ + *cis*-**H**ONO occurs readily. The calculated rate constant for the reaction at 300 K is $1.06 \times 10^6$ $cm^3$ $mol^{-1}$ $s^{-1}$, in reasonable agreement with the experimental value of $2.2 \times 10^6$ $cm^3$ $mol^{-1}$ $s^{-1}$.

## I. Introduction

It has been long known that nitrous acid (HONO) is a key reactive intermediate during the course of the chemical reactions in H/N/O-containing systems.[1−4] HONO is chemically relatively stable; it can be possibly accumulated at low temperatures.[5,6] Over the decades, the chemistry of H/N/O systems has received much attention thanks to its significant relevance to the combustion of many nitramine propellants and to the chemistry of the polluted troposphere. Accordingly, the study of HONO reactions is of great importance to our understanding of the H/N/O chemistry pertinent to the combustion of propellants and to pollution control in the troposphere.

Recently, a systematic study of HONO reactions by ab initio molecular orbital and transition-state theory (ab initio MO/TST) calculations has been performed in our laboratory. The reactions include the direct oxidation of HNO by $NO_2$ to produce HONO and NO,[6] the bimolecular decomposition of HONO,[7] the oxidation of HONO by $NO_2$ and $O_3$, and the reduction of HONO by HNO and $NH_3$. In the present paper, we report our theoretical results from the latter study. The results on the oxidation of HONO by $NO_2$ and $O_3$ will be presented in a forthcoming paper.[8]

## II. Computational Details

The structures of the reactants, products, intermediates, and transition states of the two title reactions have been fully optimized using the hybrid density functional B3LYP method (Becke's three-parameter nonlocal exchange functional[9−11] with the correlation functional of Lee et al.[12]) with the 6-311G(d,p) basis set.[13] Vibrational frequencies and zero-point energy (ZPE) corrections have been obtained at the same level of theory, and used for the subsequent TST calculations of rate constants. Each of the calculated transition states has been identified to have one imaginary frequency. All the stationary points (transition states and adjacent local minima) along the reaction paths have been connected by using the intrinsic reaction coordinate (IRC) calculations.[14] All the energies quoted and discussed in the present article include the ZPE correction.

To obtain more reliable energies, we carried out QCISD(T)/6-311G(d,p),[15] restricted closed-shell and open-shell coupled cluster RCCSD(T)/6-311G(d,p),[16] as well as G2M(RCC,MP2)[17] calculations. The G2M(RCC,MP2) method is a modification of the Gaussian-2 (G2) approach;[18] it uses B3LYP/6-311G(d,p) optimized geometries and ZPE corrections and substitutes the QCISD(T)/6-311G(d,p) calculation of the original G2 scheme by the RCCSD(T)/6-311G(d,p) calculation. The total energy in G2M(RCC,MP2) is calculated as follows:[17]

$$E[\mathrm{G2M(RCC,MP2)}] = E[(\mathrm{RCCSD(T)/6\text{-}311G(d,p)})] + \Delta E(+\mathrm{3df,2p}) + \Delta E(\mathrm{HLC}) + \mathrm{ZPE}$$

where

$$\Delta E(+\mathrm{3df,2p}) = E[\mathrm{MP2/6\text{-}311{+}G(3df,2p)}] - E[\mathrm{MP2/6\text{-}311G(d,p)}]$$

and the empirical "higher-level correction"(HLC) in millihartrees

$$\Delta E(\mathrm{HLC}) = -5.25\boldsymbol{n}_\beta - 0.19\boldsymbol{n}_\alpha$$

where $\boldsymbol{n}_\alpha$ and $\boldsymbol{n}_\beta$ are the numbers of α and β valence electrons, respectively.

All the ab initio calculations were performed using the GAUSSIAN94[19] and MOLPRO96[20] programs.

## III. Results and Discussion

**HNO + HONO Reaction.** So far, neither theoretical nor experimental work has been done on the HNO + HONO reaction. The previous ab initio and TST study of the bimolecular decomposition of HONO reveals that the reaction can proceed by a hydrogen transfer from one HONO to the O(H) atom of the second molecule accompanied by elimination of

---

* Corresponding author. E-mail: chemmcl@emory.edu.

[†] Permanent address: State Key Laboratory for Physical Chemistry of Solid Surface and Department of Chemistry, Xiamen University, Xiamen 361005, PR China.

10.1021/jp000464j CCC: $19.00

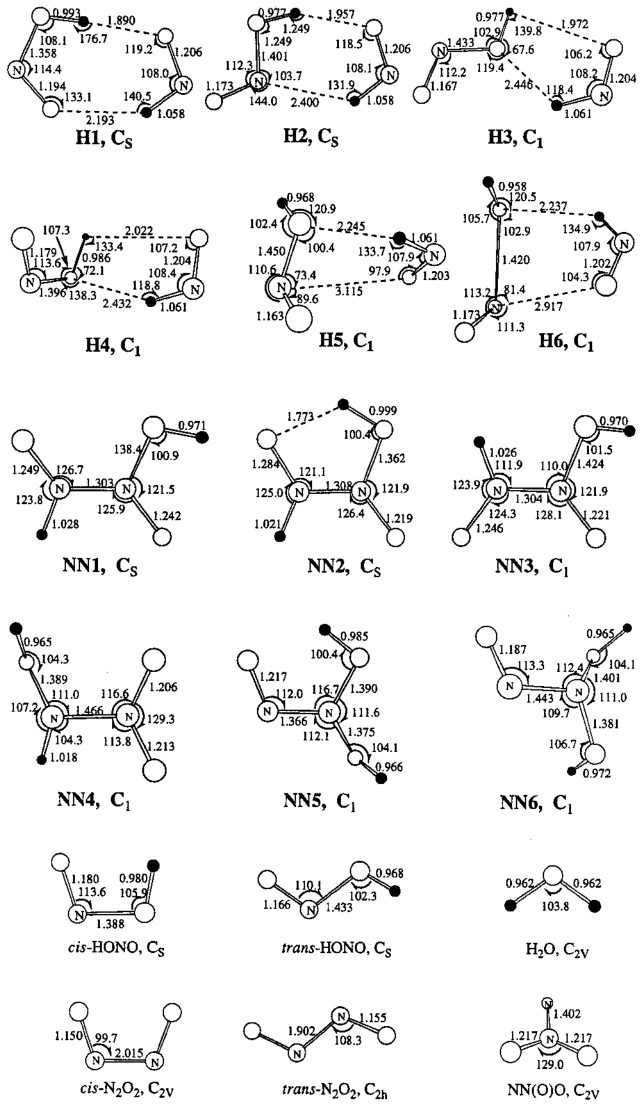

**Figure 1.** B3LYP/6-311G(d,p) optimized structures (bond lengths in angstroms, bond angles in degrees) of the reactants, intermediates, and products of the HNO + HONO reaction.

$H_2O$.[7] It can be analogously deduced that the HNO + HONO reaction proceeds in a similar manner in that the H atom of HNO directly attacks the O(H) atom of HONO, producing $H_2O$ and 2NO. This channel can be referred to as "direct elimination of $H_2O$", and can be expressed simply as

$$\mathrm{HNO + HONO \rightarrow H_2O + 2NO} \qquad (1)$$

Another possible path of this reaction is the association/elimination process:

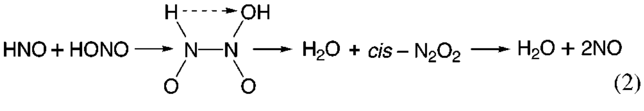

$$\mathrm{HNO + HONO \longrightarrow \underset{O\qquad O}{\overset{H\cdots\rightarrow OH}{N{-}N}} \longrightarrow H_2O + \mathit{cis}\text{-}N_2O_2 \longrightarrow H_2O + 2NO} \qquad (2)$$

which proceeds via a HN(O)N(O)OH intermediate. The products of this channel are $H_2O$ and *cis*-$N_2O_2$, which fragments to give 2NO readily. *cis*-$N_2O_2$ has been known both experimentally and theoretically to be a weakly bound dimer of NO.[21−24]

The aforementioned channels have been carefully considered in our calculations. Optimized geometries of various stable species and transition states are shown in Figures 1 and 2, respectively. Their energies are presented in Table 1.

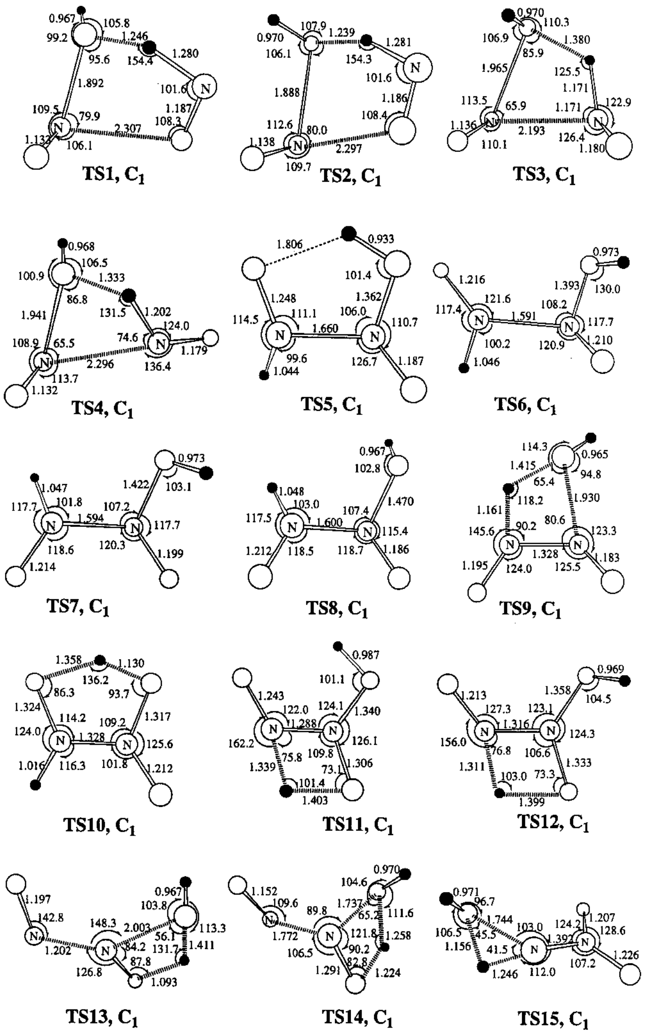

**Figure 2.** B3LYP/6-311G(d,p) optimized structures (bond lengths in angstroms, bond angles in degrees) of transition states of the HNO + HONO reaction.

*Hydrogen-Bonding Complexes of HNO and HONO.* HNO and HONO are polar molecules that are prone to form hydrogen-bonding [ONH−O(H)NO] complexes. Our recent IRC//B3LYP/6-311G(d,p) study of the bimolecular decomposition of HONO[25] reveals that some H-bonding complexes of the reactants work as precursors for the direct H-abstraction process (i.e., the direct elimination of $H_2O$) in the HONO + HONO reaction system. For the present (HNO−HONO) system, we have found six H-bonding complexes in the potential energy surface. These are **H1**−**H6** shown in Figure 1. The predicted binding energies of these complexes range from 0.8 to 3.5 kcal/mol (Table 1) at the G2M level of theory. Among these complexes, the planar, seven-member ringlike complex, **H1**, which is formed by *cis*-HONO + HNO, is the most stable. According to the structural features of these hydrogen-bonding complexes, it can be inferred that the complexes **H3**, **H4**, **H5**, and **H6** may be the precursors of the direct elimination of $H_2O$ between HNO and HONO.

*Direct Elimination of $H_2O$.* The final products of this reaction channel are $H_2O$ and 2 NO molecules. The reaction is predicted to be exothermic at all levels of theories used. The G2M-predicted exothermicity is 21.0 kcal/mol. Four transition states corresponding to the direct elimination of $H_2O$ have been located. They are labeled as **TS1**, **TS2**, **TS3**, and **TS4** in Figure 2. **TS1** and **TS4** come from HNO + *trans*-HONO, and **TS2** and **TS3** are from HNO + *cis*-HONO. At the G2M level of theory, the barrier heights of these four transition states with

**TABLE 1: Energetics[a] of Reactants, Products, Intermediates, and Transition States of the HNO+HONO System Calculated at Different Levels of Theory**

| | ZPE[b] | B3LYP/ 6-311G(d,p) | MP2/ 6-311G(d,p) | CCSD(T)/ 6-311G(d,p) | QCISD(T)/ 6-311G(d,p) | MP2/ 6-311G(3df,2p) | G2M(RCC,MP2) |
|---|---|---|---|---|---|---|---|
| *trans*-HONO+HNO | 21.4 | −336.27068[c] | −335.46705[c] | −335.51798[c] | −335.52030[c] | −335.67572[c] | −335.77410[c] |
| *cis*-HONO+HNO | 21.4 | −336.27106[c] | −335.46777[c] | −335.51854[c] | −335.52072[c] | −335.67513[c] | −335.77340[c] |
| | | −0.2 | −0.5 | −0.4 | −0.3 | +0.4 | +0.4 |
| **H1** | 23.6 | −5.4 | −4.9 | −4.8 | −4.7 | −3.5 | −3.5 |
| **H2** | 23.5 | −4.6 | −4.6 | −4.3 | −4.3 | −3.8 | −1.4 |
| **H3** | 23.2 | −3.9 | −3.9 | −3.7 | −3.7 | −2.9 | −2.7 |
| **H4** | 23.0 | −3.5 | −3.8 | −3.5 | −3.4 | −0.8 | −2.1 |
| **H5** | 22.6 | −2.5 | −3.0 | −2.8 | −2.8 | −2.2 | −2.0 |
| **H6** | 22.6 | −2.1 | −2.5 | −2.2 | −2.2 | −1.1 | −0.8 |
| **TS1** | 20.7 | +8.8 | +18.6 | +19.7 | +18.1 | +19.6 | +20.6 |
| **TS2** | 20.6 | +10.2 | +20.5 | +20.9 | +19.5 | +21.6 | +21.9 |
| **TS3** | 20.6 | +18.9 | +27.7 | +31.1 | +29.3 | +27.3 | +30.6 |
| **TS4** | 20.5 | +17.2 | +27.2 | +29.4 | +29.2 | +27.6 | +29.7 |
| **TS5** | 24.7 | +13.8 | +25.3 | +26.2 | +24.7 | +20.8 | +21.7 |
| **TS6** | 24.5 | +18.1 | +25.9 | +29.5 | +28.4 | +21.7 | +25.4 |
| **TS7** | 24.4 | +16.1 | +23.3 | +27.3 | +26.3 | +19.1 | +23.1 |
| **TS8** | 24.1 | +19.7 | +27.0 | +30.8 | +29.7 | +22.3 | +26.0 |
| **TS9** | 21.8 | +34.2 | +44.1 | +46.0 | +44.6 | +39.4 | +41.2 |
| **TS10** | 21.2 | +2.6 | +7.3 | +15.8 | +15.6 | +0.2 | +11.6 |
| **TS11** | 22.8 | +41.6 | +43.5 | +52.6 | +52.4 | +36.0 | +43.1 |
| **TS12** | 22.6 | +43.6 | +47.8 | +54.5 | +54.1 | +41.5 | +48.1 |
| **TS13** | 21.9 | +35.0 | +28.1 | +46.4 | +45.8 | +20.8 | +39.1 |
| **TS14** | 20.5 | +39.4 | +43.2 | +43.9 | +43.7 | +40.0 | +38.0 |
| **TS15** | 22.3 | +42.3 | +47.2 | +52.6 | +51.9 | +43.8 | +49.2 |
| **NN1** | 26.3 | +11.1 | +14.3 | +23.9 | +23.9 | +6.0 | +15.5 |
| **NN2** | 26.2 | +5.3 | +9.7 | +18.5 | +18.4 | +1.0 | +9.9 |
| **NN3** | 25.9 | +10.9 | +13.6 | +24.0 | +24.0 | +5.0 | +15.4 |
| **NN4** | 27.1 | −12.0 | +0.7 | +9.0 | +9.1 | −5.7 | +2.7 |
| **NN5** | 25.4 | +0.4 | +5.0 | +6.8 | +6.9 | +1.2 | +3.0 |
| **NN6** | 24.9 | +2.1 | +5.3 | +6.5 | +6.7 | +2.8 | +3.9 |
| NN(O)O+$H_2O$ | 21.1 | +26.8 | +29.5 | +29.7 | +29.9 | +28.4 | +31.8 |
| *trans*-$(NO)_2$+$H_2O$ | 20.6 | −12.5 | −15.7 | −16.4 | −15.8 | −17.0 | −18.3 |
| *cis*-$(NO)_2$+$H_2O$ | 21.1 | −16.9 | −24.8 | −20.0 | −21.0 | −21.1 | −23.3 |
| 2NO+$H_2O$ | 19.1 | −21.3 | −22.9 | −26.8 | −26.4 | −20.1 | −21.0 |

[a] Relative energies in kcal/mol with respect to *trans*-HONO + HNO. [b] Zero-point energy corrections (kcal/mol), calculated at the B3LYP/6-311G(d,p) level. [c] Total energies are given in hartrees.

respect to the corresponding free reactants are 20.6, 21.5, 30.2, and 29.7 kcal/mol, respectively. IRC//B3LYP/6-311 G(d,p) calculations reveal that **TS1**, **TS2**, **TS3**, and **TS4** actually derive from the 4 H-bonding complexes, that is, **H5**, **H6**, **H4**, and **H3**, respectively. This confirms the inference made in the preceding paragraph. The IRC calculations also indicate that both **TS1** and **TS2** lead to the direct products of $H_2O$ + 2NO, whereas **TS3** and **TS4** result in the formation of *cis*-$N_2O_2$ and *trans*-$N_2O_2$ intermediates, respectively. It is known that *trans*-$N_2O_2$ is unstable, and *cis*-$N_2O_2$ is very weakly bound with a dimerization energy of 2−4 kcal/mol (experimental value[21,22]). Our G2M calculations predict a metastable *trans*-$N_2O_2$, and a dimerization energy of 2.3 kcal/mol for *cis*-$N_2O_2$, in good accordance with the experimental observations.

*Association−Elimination Mechanism.* Topologically there should exist four isomers of N−N bonding HN(O)N(O)OH formed by the association of HNO with *cis*- and *trans*-HONO, as depicted in Scheme 1. However, only three conformers have been found in the potential energy surface (PES) of HN(O)N(O)OH. They are **NN1**, **NN2**, and **NN3** in Figure 1, corresponding to (a), (b), and (c) in the scheme. Optimization with an initial geometry like that given in Scheme 1 (c) or (d) converges to a common, nonplanar conformer, **NN3**. All three conformers are formed endothermically with respect to free HNO and HONO. Among these conformers, **NN2** is the lowest in energy because of the existence of intramolecular hydrogen bonding. Note that the distance between the O atom of the HNO group and the H atom of the HONO group in **NN2** is only 1.773 Å, even shorter than the shortest H-bonding distance in the H-bonding [ONH−O(H)NO] complexes (1.890 Å in **H1**).

**SCHEME 1**

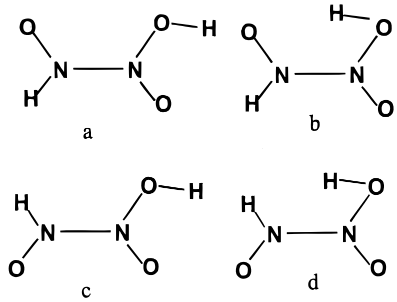

Four transition states that connect the HN(O)N(O)OH conformers and the reactants are shown in Figure 2. **TS5** leads to the formation of **NN2** from HNO + *trans*-HONO. **TS6** leads to the formation of **NN1** from HNO + *cis*-HONO. Both **TS7** and **TS8**, which derive from *cis*- and *trans*-HONO reactions, respectively, result in **NN3**. At the G2M level of theory, the barrier heights for **TS5**−**TS8** are, respectively, 21.7, 25.0, 22.7, and 26.0 kcal/mol; these values are comparable with those for direct elimination of $H_2O$.

Among the three conformers of HN(O)N(O)OH, only **NN3** can eliminate $H_2O$ by reaction 2, whereas for **NN1** and **NN2**, intramolecular H-transfer is required to reach a geometry that can undergo further dehydration. The dehydration of **NN3** proceeds by transition state, **TS9**, which is higher than **NN3** by

**TABLE 2: Molecular and Transition-State Parameters of the Reactants, and Transition States of the HNO + HONO and $NH_3$ + HONO Reactions, Used for TST Calculations of Rate Constants [Calculated at the B3LYP/6-311G(d,p) Level]**

| species | $I_I$ ($10^{-14}$g cm$^2$) | frequencies (cm$^{-1}$) |
|---|---|---|
| *trans*-HONO | 8.9, 67.4, 76.3 | 591, 618, 834, 1298, 1793, 3776 |
| *cis*-HONO | 10.1, 63.2, 73.4 | 638, 719, 892, 1338, 1721, 3584 |
| HNO | 1.5,19.7, 21.2 | 1577, 1674, 2828 |
| $NH_3$ | 2.9, 2.9, 4.5 | 1069, 1681, 1682, 3464, 3583, 3583 |
| | | HNO + HONO reaction |
| **TS1** | 107.3, 218.5, 300.2 | 1234*i*, 132, 198, 350, 380, 400, 568, 630, 663, 784, 1332, 1612, 1711, 1939, 3796 |
| **TS2** | 119.0, 223.4, 306.2 | 1229*i*, 129, 191, 340, 386, 391, 585, 637, 659, 796, 1291, 1627, 1720, 1911, 3752 |
| | | $NH_3$ + HONO reaction |
| **TS1′** | 95.7, 124.1, 197.3 | 1231*i*, 271, 294, 343, 450,458, 620, 640, 646, 755, 793, 1480, 1666, 1702, 1905, 3505, 3627, 3816 |
| **TS2′** | 96.0, 125.3, 198.8 | 1227*i*, 267, 271, 335, 454, 490, 603, 643, 665, 777, 792, 1477, 1670, 1703, 1873, 3504, 3626, 3790 |
| **TS8′** | 66.4, 148.4, 210.1 | 465*i*, 220, 342, 363, 405, 504, 827, 1043, 1310, 1326, 1482, 1604, 1625, 1687, 2312, 2664, 3492, 3585 |

**TABLE 3: Fitted Expressions for Rate Constants[a] ($cm^3\ mol^{-1}\ s^{-1}$) and Apparent Activation Energies (kcal/mol) of the HNO + HONO Reactions**

| reaction | 300−3000 K 3-parameter fitting | 300 K | 300−1000 K 2-parameter fitting | $E_a$ |
|---|---|---|---|---|
| *trans*-HONO + HNO, $k_1$ | $1.72 \times 10^{-3} T^{4.13}\exp(-8350/T)$ | $3.01 \times 10^{-5}$ | $2.55 \times 10^{10}\exp(-10500/T)$ | 20.9 |
| *cis*-HONO + HNO, $k_2$ | $1.76 \times 10^{-3} T^{4.18}\exp(-8850/T)$ | $7.86 \times 10^{-6}$ | $3.63 \times 10^{10}\exp(-11000/T)$ | 21.9 |

[a] Eckart tunneling correction was used to compute the rate constants (see ref 27).

25.8 kcal/mol and higher than the HNO + *trans*-HONO reactants by 41.4 kcal/mol at the G2M level. For **NN2**, H-transfer may proceed from HONO to HNO via **TS10** to the intermediate **NN4** or from HNO to HONO via **TS11** to **NN5**. The barrier height for the former process is very low (1.7 kcal/mol), whereas for the latter the barrier height is very high, 33.2 kcal/mol. The reactions from free HNO + *trans*-HONO to **NN4** and **NN5** are nearly thermoneutral, 2.7 kcal/mol for the former and 3.0 kcal/mol for the latter. For **NN1**, the H-transfer from HNO to HONO via **TS12** results in the intermediate **NN6**, which is only ~1.0 kcal/mol higher than **NN4** and **NN5**. This H-transfer process has a barrier height of 22.6 kcal/mol, but **TS12** is higher than the reactants by 48.1kcal/mol. **NN4**, **NN5**, and **NN6** are ready for further dehydration, as suggested by their geometries.

The dehydration of **NN4** gives rise to N═N(O)O, which is a high-energy isomer of $N_2O_2$. This process goes through a transition state, **TS15**, with a barrier height (46.5 kcal/mol) too high to be important; it is also highly endothermic. The dehydration of **NN5** proceeds via a transition state, **TS13**, with a barrier height of 36.1 kcal/mol, resulting in the formation of *trans*-$N_2O_2$. The dehydration of **NN6** also produces *trans*-$N_2O_2$. The corresponding transition state **TS14** has a barrier height of 34.1 kcal/mol.

All the aforementioned reaction channels are schematically shown in Figure 3. Clearly, for the reduction of HONO by HNO via HN(O)N(O)OH, it has to pass through transition states with very high barriers for the dehydration process. Accordingly, the association/elimination reaction involving HN(O)N(O)OH intermediates cannot compete effectively with the direct dehyration processes described above.

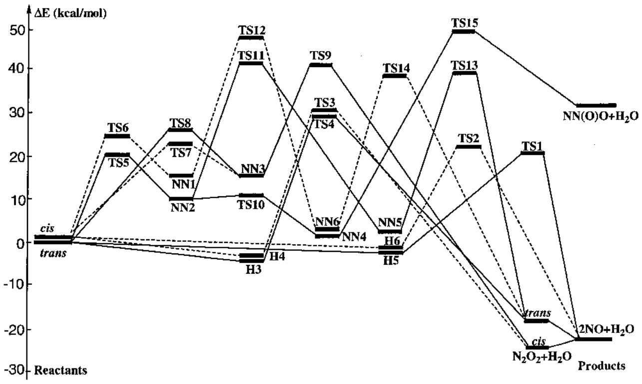

**Figure 3.** Energy diagram for the potential energy surface of the HNO + HONO reaction calculated in the framework of the G2M(RCC, MP2)//B3LYP/6-311G(d,p) approach. Solid lines connect the *trans*-HONO related channels; dotted lines connect the *cis*-HONO related channels.

*TST Calculations of Rate Constants.* We have shown in our ab initio MO calculations that the key channels responsible for the HNO + HONO are those taking place by direct elimination of $H_2O$ via hydrogen-bonding complexes. These are the reactions that go through **TS1**−**TS4**. As the barrier heights of **TS3** and **TS4** are higher than those of **TS1** and **TS2** by about 9−10 kcal/mol, we only consider the channels occurring via **TS1** and **TS2** in our rate constant calculations using TST.[26] The barrier heights calculated at the G2M level (given in Table 1) and the B3LYP/6-311G(d,p) molecular parameters of the reactants and transition states (Table 2) were used in our TST calculations. A complete summary of molecular parameters is presented in Appendix A. We used the conventional TST method with Eckart tunneling corrections described earlier.[27] The rate constant expressions obtained by 2- and 3-parameter fitting are presented in Table 3. For the reaction HNO + *trans*-HONO → **TS1** → 2NO + $H_2O$, 2-parameter fitting in the 300−1000 K temperature range gives an A factor of $2.55 \times 10^{10}$ $cm^3\ mol^{-1}\ s^{-1}$ and an apparent activation energy of 20.9 kcal/mol. The reaction HNO + *cis*-HONO → **TS2** → 2NO + $H_2O$ is slightly slower, with an A factor of $3.63 \times 10^{10}$ $cm^3\ mol^{-1}\ s^{-1}$ and an apparent activation energy of 21.9 kcal/mol.

**HONO + $NH_3$ Reaction.** For the $NH_3$ + HONO reaction, the experimental work of Kaiser and Japar gave an upper limit for the rate constant ($\leq 9.04 \times 10^6$ $cm^3\ mol^{-1}\ s^{-1}$),[28] which is at least 4 orders slower than the $NH_3$ + $HNO_3$ reaction. Unfortunately, the products of the reaction were not clearly identified in their paper. The recent ab initio study of the bimolecular reaction of $NH_3$ with $HNO_3$ suggested the following two major channels,[29]

$$NH_3 + HNO_3 \rightarrow H_2NNO_2 + H_2O \tag{3}$$

$$NH_3 + HNO_3 \rightarrow H_2NONO + H_2O \tag{4}$$

and predicted that both channels have approximately the same barrier, 46 kcal/mol. We expect that a similar mechanism may

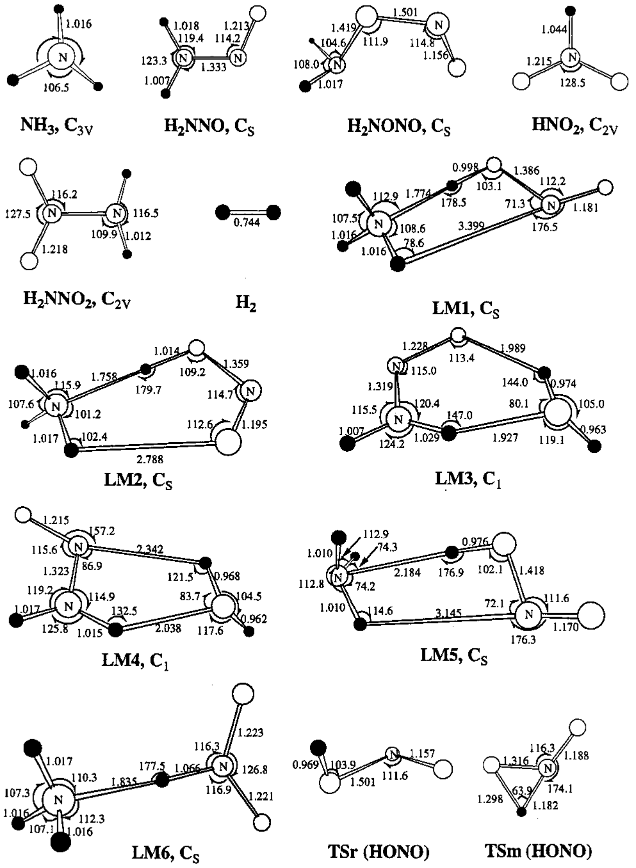

**Figure 4.** B3LYP/6-311G(d,p) optimized structures (bond lengths in angstroms, bond angles in degrees) of NH, intermediates, and products of the $NH_3$ + HONO reaction.

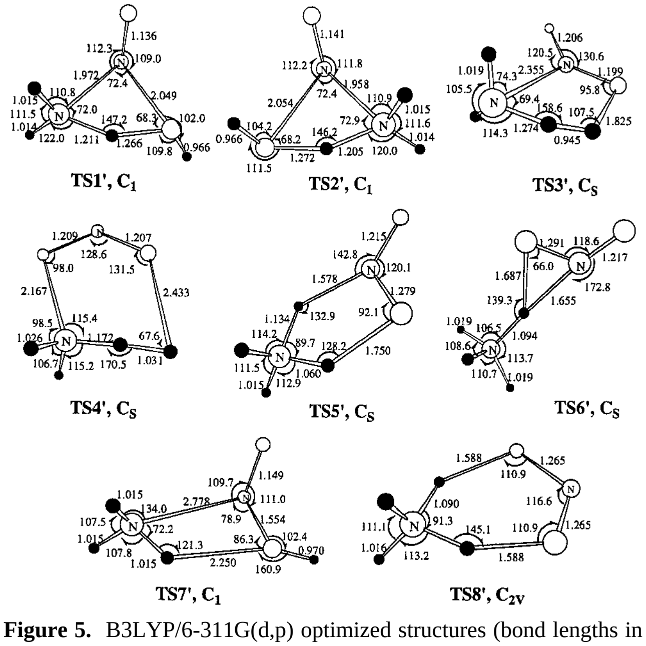

**Figure 5.** B3LYP/6-311G(d,p) optimized structures (bond lengths in angstroms, bond angles in degrees) of transition states of the $NH_3$ + HONO reaction.

exist in the $NH_3$ + HONO reaction system, viz.

$$NH_3 + HONO \rightarrow H_2NNO + H_2O \qquad (5)$$

Another possible reaction may take place by $H_2$ elimination,

$$NH_3 + HONO \rightarrow H_2NONO\ (\text{or } H_2NNO_2) + H_2 \qquad (6)$$

**TABLE 4: Energetics[a] of Reactants, Products, Intermediates, and Transition States of the $NH_3$ + HONO System Calculated at Different Levels of Theory**

| species | ZPE[b] | B3LYP/ 6-311G(d,p) | G2M (RCC,MP2) |
|---|---|---|---|
| $NH_3$ + *trans*-HONO | 34.2 | −262.33780[c] | −261.91684[c] |
| $NH_3$ + *cis*-HONO | 34.2 | −262.33819[c]<br>(−0.2) | −261.91613[c]<br>(+0.4) |
| **TS1′** | 32.8 | 24.6 | 33.4 |
| **TS2′** | 32.8 | 26.0 | 34.9 |
| **TS3′** | 29.7 | 97.4 | 101.6 |
| **TS4′** | 28.2 | 92.9 | 97.7 |
| **TS5′** | 35.8 | 11.0 | 15.4 |
| **TS6′** | 36.0 | 21.3 | 21.3 |
| **TS7′** | 34.2 | 9.6 | 9.3 |
| **TS8′** | 35.4 | 0.3 | 5.9 |
| **LM1** | 36.5 | −11.5 | −8.2 |
| **LM2** | 36.3 | −11.4 | −7.1 |
| **LM3** | 36.7 | −17.5 | −13.8 |
| **LM4** | 36.2 | −15.7 | −12.8 |
| **LM5** | 35.5 | −2.6 | −0.2 |
| **LM6** | 37.2 | −4.1 | −0.0 |
| $H_2NONO + H_2$ | 29.1 | 46.5 | 49.5 |
| $H_2NNO_2 + H_2$ | 30.9 | 23.8 | 29.7 |
| $NH_3 + HNO_2$ | 35.3 | 7.3 | 8.7 |
| $H_2NNO + H_2O$ | 35.5 | −8.8 | −7.1 |

[a] Relative energies in kcal/mol with respect to $NH_3$ + *trans*-HONO. [b] Zero-point energy corrections (kcal/mol), calculated at the B3LYP/6-311G(d,p) level. [c] Total energies are given in hartrees.

These reactions as well as the other possibilities have been carefully considered in our calculations. Optimized geometries of various species and stationary points for the $NH_3$ + HONO reaction are shown in Figures 4 and 5. The total energy of the reactants and the relative energies of the transition states, intermediates, and products calculated at the B3LYP/6-311G(d,p) and G2M(RCC, MP2) level of theory, as well as the values of ZPE corrections are summarized in Table 4. The schematic energy diagram for the potential energy surface of the reaction under consideration is illustrated in Figure 6.

*Potential Energy Surface.* Our B3LYP//IRC//G2M calculations for the reaction of ammonia with nitrous acid reveal eight possible distinct pathways (**I**−**VIII**) that lead to the formation of four different sets of final products, $H_2NNO + H_2O$, $H_2NNO_2 + H_2$, $H_2NONO + H_2$, and $NH_3 + HNO_2$. They are

$$\text{I. } NH_3 + trans\text{-HONO} \rightarrow (\mathbf{TS1'}) \rightarrow H_2NNO + H_2O$$

$$\text{II. } NH_3 + cis\text{-HONO} \rightarrow (\mathbf{TS2'}) \rightarrow H_2NNO + H_2O$$

$$\text{III. } NH_3 + trans\text{-HONO} \rightarrow (\mathbf{TS3'}) \rightarrow H_2NNO_2 + H_2$$

$$\text{IV. } NH_3 + cis\text{-HONO} \rightarrow (\mathbf{TS4'}) \rightarrow H_2NONO + H_2$$

$$\text{V. } NH_3 + trans\text{-HONO} \rightarrow (\mathbf{TS5'}) \rightarrow NH_3 + HNO_2$$

$$\text{VI. } NH_3 + trans\text{-HONO} \rightarrow (\mathbf{TS6'}) \rightarrow NH_3 + HNO_2$$

$$\text{VII. } NH_3 + trans\text{-HONO} \rightarrow (\mathbf{TS7'}) \rightarrow NH_3 + cis\text{-HONO}$$

$$\text{VIII. } NH_3 + cis\text{-HONO} \rightarrow (\mathbf{TS8'}) \rightarrow NH_3 + cis\text{-HONO}$$

Let us consider these channels in detail. As can be seen from the PES presented in Figure 6, the channel **I**, $NH_3$ + *trans*-HONO → **LM1** → **TS1′** → **LM3** → $H_2NNO + H_2O$, proceeds by abstraction of a hydrogen atom from $NH_3$ by the O(H) atom of *trans*-HONO, followed by breaking the O(H)−N bond of HONO and the association of $H_2N$ with NO. This reaction is exothermic by 7.1 kcal/mol and has an activation barrier of 33.4 kcal/mol. Interestingly, the hydrogen-bonding intermediate,

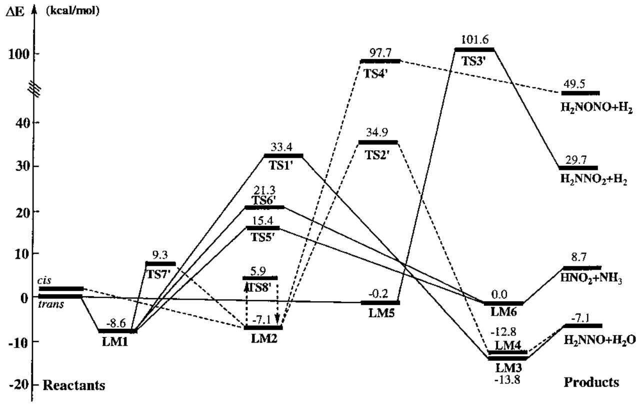

**Figure 6.** Energy diagram for the potential energy surface of the $NH_3$ + HONO reaction calculated in the framework of the G2M(RCC,-MP2)//B3LYP/6-311G(d,p) approach. Solid lines connect the *trans*-HONO related channels; dotted lines connect the *cis*-HONO related channels.

**LM1**, has been found to work as a precursor of the H-abstraction transition state, **TS1′**. Following **TS1′** in the reaction path, there exists another intermediate, **LM3**, which is a H-bonding complex of the products, $H_2NNO + H_2O$. With $NH_3$ + *cis*-HONO as the reactants, we have a similar channel (**II**), $NH_3$ + *cis*-HONO → **LM2** → **TS2′** → **LM4** → $H_2NNO + H_2O$, which is exothermic by 7.5 kcal/mol. The barrier height was found to be 34.5 kcal/mol, slightly higher than that of channel **I**. The intermediates, **LM2** and **LM4**, in this channel are H-bonding complexes of the reactants and the products, respectively. **LM4** has a five-member ring structure with hydrogen-bonding involving H···O and H···N, whereas **LM3** of channel **I** has a six-member ring structure with two H···O bonds. The hydrogen-bonding interaction between $H_2O$ and $H_2NNO$ in **LM3** is stronger than that in **LM4**, as indicated by the lower total energy of **LM3** and the shorter H···O bond lengths in **LM3**. Channel **III**, $NH_3$ + *trans*-HONO → **LM5** → **TS3′** → $H_2NNO_2 + H_2$, goes through a van der Waals intermediate **LM5** and transition state, **TS3′**. A similar channel, **IV**, that involves *cis*-HONO via the intermediate **LM2** and transition state **TS4′**, however, leads to a different product, $H_2NONO$. Both channels **III** and **IV** are not expected to be practically important in the $NH_3$ + HONO reaction, because they are sufficiently endothermic and require much higher activation energies (101.6 kcal/mol for channel **III** versus 97.3 kcal/mol for channel **IV**). Reaction channels **V**, $NH_3$ + *trans*-HONO → **LM1** → **TS5′** → **LM6** → $HNO_2 + NH_3$, and **VI**, $NH_3$ + *trans*-HONO → **LM1** → **TS6′** → **LM6** → $HNO_2 + NH_3$, are endothermic by 8.6 kcal/mol; they lead to the formation of $HNO_2$ and $NH_3$ products via transition states **TS5′** and **TS6′**, respectively. The barrier heights of channels **V** and **VI** are 15.4 and 21.3 kcal/mol, respectively. It is worth noting that both reaction channels have a common prereaction intermediate (**LM1**), a common postreaction intermediate (**LM6**), and common products. However, channel **V** involves H-atom exchange between $NH_3$ and *trans*-HONO, whereas channel **VI** is an $NH_3$-catalyzed intramolecular H-transfer process within HONO. A similar unimolecular isomerization process, *trans*-HONO → $HNO_2$, occurs via transition state, **TSm** (see Figure 4), with an activation energy of 55.2 kcal/mol (see Figure 7). [This G2M prediction is in good agreement with the previous prediction of 55.2 kcal/mol obtained by Jursic[30] at the B3LYP/6-311G(3df, 3dp) level of theory.] Hence, the presence of $NH_3$ promotes the isomerization of *trans*-HONO into $HNO_2$ by reducing the energy barrier by as much as 34 kcal/mol. Reaction channel **VII**, $NH_3$ + *trans*-HONO → **LM1** → **TS7′** → **LM2** → $NH_3$ + *cis*-HONO, corresponds to the trans−cis isomerization of HONO in the presence of $NH_3$. Indeed, the transition state, **TS7′**, is simply a H-bonding complex of $NH_3$ with the rotational transition state (**TSr**) for the trans−cis isomerization of HONO. The barrier height of this channel is 9.3 kcal/mol with respect to free $NH_3$ + *trans*-HONO, and 17.9 kcal/mol with respect to **LM1**. For the trans−cis isomerization of an isolated HONO molecule, our G2M calculations predict a rotational transition state, **TSr** (see Figure 4), which is higher than *trans*-HONO by 10.5 kcal/mol (see Figure 7). It is clear that the presence of $NH_3$ somewhat hinders the trans−cis isomerization of HONO. Besides the aforementioned transition states (**TS1′**−**TS7′**), we also located a transition state, **TS8′**, that connects the two equivalent isomers of **LM2** in the potential energy surface of the ($NH_3$ + *cis*-HONO) system. This reaction path, channel **VIII**, describes a reversible gas-phase reaction $NH_3$ + *cis*-HONO ⇔ $NH_2$H + *cis*-HONO, which was studied experimentally by infrared diode laser spectroscopy.[31] The activation energy of this reversible exchange reaction predicted at the G2M level of theory is only 5.5 kcal/mol.

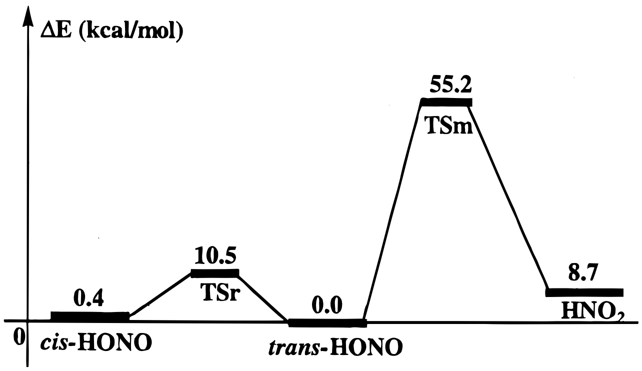

**Figure 7.** Energy diagram for the potential energy surface of the isomerization of an isolated HONO calculated in the framework of the G2M(RCC,MP2)//B3LYP/6-311G(d,p) approach.

*Calculation of Rate Constants.* The rate constants for the $NH_3$ + *trans*-HONO reaction via **TS1′** (channel **I**) and for the $NH_3$ + *cis*-HONO reaction via **TS2′** (channel **II**) have been calculated by TST with Eckart tunneling corrections, using the activation barriers and molecular parameters given in Tables 4 and 2, respectively. A complete summary of the molecular parameters for the system is presented in Appendix B. Two-parameter fitting in the 300−1000 K temperature range gives the following Arrhenius expressions (in $cm^3\ mol^{-1}\ s^{-1}$) for channels **I** and **II**:

$$k_{\mathrm{I}} = 3.16 \times 10^{10} \exp(-16800/T)$$

$$k_{\mathrm{II}} = 4.06 \times 10^{10} \exp(-17400/T)$$

with the corresponding apparent activation energies of 33.3 and 34.5 kcal/mol, respectively. The 3-parameter expressions also in $cm^3\ mol^{-1}\ s^{-1}$ fitted in the temperature range 300−3000 K are:

$$k_{\mathrm{I}} = 9.64 \times 10^{-4}\, T^{4.24} \exp(-14600/T)$$

$$k_{\mathrm{II}} = 1.08 \times 10^{-3}\, T^{4.26} \exp(-15200/T)$$

At 300 K, the calculated rate constants for the two channels are $3.36 \times 10^{-14}$ and $5.62 \times 10^{-15}$ $cm^3\ mol^{-1}\ s^{-1}$, respectively, which are significantly lower than the upper limit reported by Kaiser and Japar,[28] $9 \times 10^{6}$ $cm^3\ mol^{-1}\ s^{-1}$. We have performed TST calculations for channel **VIII**, which has the lowest barrier height. The calculated rate constant for this reversible exchange reaction at 300K is $1.06 \times 10^6$ $cm^3$ $mol^{-1}$ $s^{-1}$, in good accordance with the experimental value of $2.2 \times 10^6$ $cm^3$ $mol^{-1}$ $s^{-1}$. Two-parameter fitting in the 300−1000 K temperature range gives the rate constant expression, $k_{VIII} = 1.42 \times 10^{10} \exp(-2930/T)$ $cm^3$ $mol^{-1}$ $s^{-1}$, with the apparent activation energy of 5.8 kca/mol.

## IV. Concluding Remarks

The gas-phase reactions of HONO with HNO and $NH_3$ have been investigated using ab initio MO and TST calculations. The main reaction channels for the HNO + *trans*-HONO and HNO + *cis*-HONO reactions are those proceeding via five-member-ring transition states, leading to the elimination of $H_2O$. The corresponding barrier heights center around 21 kcal/mol. The reaction is exothermic by 21 kcal/mol. TST calculations with tunneling corrections gave the rate constants $k_1 = 1.72 \times 10^{-3} T^{4.13}\exp(-8350/T)$ and $k_2 = 1.76 \times 10^{-3} T^{4.18}\exp(-8850/T)$ $cm^3$ $mol^{-1}$ $s^{-1}$ for the two reaction channels, respectively. Other channels that go through the HN(O)N(O)OH intermediates have been shown to require much higher activation energies for further dehydration and, therefore, are unfavorable.

**Appendix A: Overall Moments of Inertia ($10^{-40}$ g $cm^2$), and Vibrational Frequencies ($cm^{-1}$) for Various Species Involved in the HONO + HNO Reaction Computed at B3LYP/6-311G(d,p)**

| species | $I_a, I_b, I_c$ | frequencies |
|---|---|---|
| *trans*-HONO | 8.9, 67.4, 76.3 | 591, 618, 834, 1298, 1793, 3776 |
| *cis*-HONO | 10.1, 63.2, 73.4 | 638, 719, 892, 1338, 1721, 3584 |
| HNO | 1.5, 19.7, 21.2 | 1577, 1674, 2828 |
| **H1** | 81.5, 308.5, 390.0 | 83, 147, 166, 179, 244, 460, 701, 901, 981, 1423, 1591, 1670, 1677, 2979, 3331 |
| **H2** | 65.2, 381.3, 446.5 | 89, 103, 141, 165, 221, 385, 675, 787, 893, 1409, 1595, 1675, 1772, 2961, 3596 |
| **H3** | 42.3, 489.6, 498.5 | 41, 82, 107, 148, 236 390, 636, 783, 847, 1355, 1592, 1672, 1790, 2921, 3615 |
| **H4** | 58.5, 431.0, 470.6 | 31, 82, 110, 162, 238, 361, 636, 823, 896, 1360, 1593, 1672, 1724, 2918, 3472 |
| **H5** | 92.4, 314.1, 352.6 | 46, 51, 75, 150, 179, 276, 578, 607, 805,1283, 1593, 1675, 1800, 2921, 3772 |
| **H6** | 77.9, 337.6, 398.6 | 53, 64, 119, 132, 192, 324, 576, 690, 839, 1308, 1589, 1679, 1746, 2925, 3605 |
| **TS1** | 107.3, 218.5, 300.2 | 1234*i*, 132, 198, 350, 380, 400, 568, 630, 663, 784, 1332, 1612, 1711, 1939, 3796 |
| **TS2** | 119.0, 223.4, 306.2 | 1229*i*, 129, 191, 340, 386, 391, 585, 637, 659, 796, 1291, 1627, 1720, 1911, 3752 |
| **TS3** | 118.3, 225.7, 309.5 | 1225*i*, 39, 190,270, 349, 438, 535, 569, 656, 733, 1364, 1726, 1888, 1921, 3750 |
| **TS4** | 95.8, 284.6, 357.3 | 1352*i*, 99, 158, 233, 341, 429, 524, 559, 662, 756, 1320, 1730, 1763, 1951, 3791 |
| **TS5** | 73.2, 194.9, 264.6 | 399*i*, 205, 268, 455, 591, 694, 725, 864, 1077, 1347, 1417, 1476, 1702, 3121, 3328 |
| **TS6** | 76.7, 199.9, 272.2 | 478*i*, 194, 277, 389, 518, 577, 625, 825, 1078, 1345, 1463, 1513, 1580, 3095, 3686 |
| **TS7** | 77.2, 207.9, 278.1 | 430*i*, 143, 191, 294, 488, 537, 612, 868, 958, 1260, 1447, 1538, 1649, 3063, 3780 |
| **TS8** | 75.2, 207.1, 276.7 | 428*i*, 180, 274, 358, 514, 563, 588, 898, 985, 1336, 1451, 1535, 1615, 3090, 3687 |
| **TS9** | 113.0, 177.2, 280.7 | 1376*i*, 158, 234, 275, 452, 555, 590, 638, 841, 931, 1217, 1643, 1678, 2212, 3825 |
| **TS10** | 67.8, 166.9, 234.3 | 1023*i*, 293, 425, 545, 623, 774, 814, 1010, 1053, 1189, 1343, 1456, 1634, 2188, 3549 |
| **TS11** | 84.4, 161.5, 246.0 | 1839*i*, 277, 260, 396, 494, 545, 828, 950, 1030, 1230, 1384, 1513, 1598, 2099, 3479 |
| **TS12** | 87.5, 169.5, 254.5 | 1813*i*, 177, 197, 294, 357, 547, 810, 898, 1076, 1192, 1299, 1460, 1609, 2120, 3741 |
| **TS13** | 73.5, 262.0, 332.9 | 1078*i*, 160, 199, 371, 466, 481, 590, 702, 772, 1142, 1194, 1344, 1867, 2259, 3794 |
| **TS14** | 84.5, 222.1, 276.7 | 1031*i*, 75, 223, 285, 300, 451, 522, 724, 759, 934, 1205, 1307, 1857, 1951, 3772 |
| **TS15** | 71.1, 201.6, 269.3 | 1590*i*, 152, 255, 404, 432, 590, 692, 769, 916, 1005, 1326, 1370, 1652, 2285, 3760 |
| **NN1** | 75.3, 176.5, 251.8 | 276, 324, 341, 399, 529, 702, 714, 853, 1249, 1326, 1395, 1523, 1677, 3363, 3744 |
| NN2 | 72.2, 170.3, 242.5 | 282, 342, 442, 551, 573, 694, 759, 881, 1176, 1335, 1373, 1519, 1699, 3242, 3470 |
| **NN3** | 74.9, 183.7, 258.2 | 194, 245, 317, 350, 496, 639, 662, 982, 1119, 1299, 1419, 1585, 1683, 3377, 3756 |
| **NN4** | 72.5, 183.4, 248.3 | 174, 297, 380, 510, 614, 774, 835, 1024, 1097, 1362, 1383, 1503, 1723, 3510, 3798 |
| **NN5** | 78.4, 171.4, 241.9 | 213, 350, 379, 431, 488, 508, 699, 838, 1088, 1139, 1425, 1446, 1570, 3458, 3375 |
| **NN6** | 83.6, 175.9, 246.8 | 216, 276,323, 357, 367, 494, 618, 785, 977, 1075, 1352, 1441, 1692, 3673, 3800 |
| NN(O)O | 60.0, 64.1, 124.2 | 387, 622, 658, 889, 1296, 1557 |
| *trans*-$N_2O_2$ | 14.7, 183.0, 197.7 | 88, 241, 270, 779, 1775, 1914 |
| *cis*-$N_2O_2$ | 31.9, 123.9, 155.7 | 249, 304, 404, 713, 1781, 1962 |
| NO | 16.4, 16.4 | 1984 |
| $H_2O$ | 1.1, 1.9, 3.0 | 1640, 3819, 3906 |

**Appendix B: Overall Moments of Inertia ($10^{-40}$ g $cm^2$), and Vibrational Frequencies ($cm^{-1}$) for Various Species Involved in the $NH_3$ + HONO Reaction Computed at B3LYP/6-311G(d,p)**

| species | $I_a, I_b, I_c$ | frequencies |
|---|---|---|
| *trans*-HONO | see Appendix A | |
| *cis*-HONO | see Appendix A | |
| $NH_3$ | 2.9, 2.9, 4.5 | 1069, 1681, 1682, 3464, 3583, 3583 |
| **TS1′** | 95.7, 124.1, 97.3 | 1231*i*, 271, 294, 343, 450,458, 620, 640, 646, 755, 793, 1480, 1666, 1702, 1905, 3505, 3627, 3816 |
| **TS2′** | 96.0, 125.3, 198.8 | 1227*i*, 267, 271, 335, 454, 490, 603, 643, 665, 777, 792, 1477, 1670, 1703, 1873, 3504, 3626, 3790 |
| **TS3′** | 73.6, 153.7, 222.9 | 1167*i*, 145, 291,314, 417,428, 650, 820, 847,869, 1211, 1335, 1365, 1576, 1688, 1782, 3460,3557 |
| **TS4′** | 73.6, 125.6, 194.8 | 673*i*, 92, 227, 269, 294, 427, 551, 722, 782, 862, 1156, 1276, 1432, 1556, 1574, 1617, 3399, 3511 |
| **TS5′** | 44.0, 203.8, 243.0 | 460*i*, 221, 300, 416, 485, 514, 811, 1006, 1271, 1415, 569, 1600, 1619, 1661, 2095, 2934, 3526, 3612 |
| **TS6′** | 38.0, 239.4, 272.8 | 772*i*, 79, 168, 173, 303, 387, 790, 1136, 1313, 1362, 1504, 1550, 1656, 1701, 2454, 3448, 3562, 3562 |
| **TS7′** | 78.9, 196.3, 255.2 | 559*i*, 71, 87, 103, 144, 226, 336, 500, 767, 1035, 1062, 1665, 1687, 1836, 3467, 3594, 3596, 3762 |
| **TS8′** | 66.4, 148.4, 210.1 | 465*i*, 220, 342, 363, 405, 504, 827, 1043, 1310, 1326, 1482, 1604, 1625, 1687, 2312, 2664, 3492, 3585 |
| **LM1** | 26.5, 315.4, 337.4 | 41, 86, 137, 247.0, 334, 387, 719, 925, 1054, 1138, 1508, 1673, 1674, 1748, 3190, 3473, 3589, 3592 |
| **LM2** | 63.7, 206.7, 265.9 | 62, 95, 171, 252, 344, 396, 713, 1005, 1107, 1130, 1485, 1656, 1677, 1679, 2952, 3468, 3586, 3591 |
| **LM3** | 68.0, 182.8, 248.2 | 164, 185, 218, 274, 348, 502, 662, 706, 867, 1160,1278,1562, 1625, 1660,3276, 3625,3677, 3866 |
| **LM4** | 40.6, 267.1, 305.5 | 103, 122, 203, 227, 264, 487, 520, 647, 815, 1152, 1259, 1573, 1612, 1648, 3426, 3604, 3748, 3876 |
| **LM5** | 29.8, 347.1, 372.2 | 50, 63, 106, 138, 323, 367, 606, 653, 770, 865, 1375, 1636, 1638, 1779, 3516, 3596, 3677, 3680 |
| **LM6** | 68.3, 241.2, 305.0 | 23, 45, 197, 213, 385, 433, 790, 1140, 1258, 1391, 1599, 1669, 1675, 1692, 2860, 3471, 3587, 3588 |
| $H_2NNO$ | 10.3, 65.6, 75.9 | 187, 631, 723, 1092, 1223, 1580, 1610, 3455, 3697 |
| $H_2NNO_2$ | 66.8, 71.1, 136.9 | 427,573, 628, 729, 810,1014, 1240,1387,1612,1687, 3526, 3658 |
| $H_2NONO$ | 15.9, 173.1, 184.5 | 191, 259, 377, 499, 760, 1009, 1168, 1337, 1666, 1806, 3452, 3539 |
| $HNO_2$ | 7.8, 64.1, 71.9 | 801, 1069, 1407, 1542, 1677, 3146 |
| $H_2O$ | 1.1, 1.9, 3.0 | 1640, 3810, 3906 |
| $H_2$ | 0.5, 0.5 | 4419 |

In the $NH_3$ + HONO system, the reversible exchange reaction $N\mathbf{H}_3$ + *cis*-HONO ⇔ $\mathbf{H}_2N\mathbf{H}$−O(H)NO ⇔ $N\mathbf{H}_2H$ + *cis*-**H**ONO has the lowest activation energy, 5.5 kcal/mol. The channels leading to the production of $H_2NNO$ and $H_2O$ require high activation energies (33−35 kcal/mol); they may become important only at high temperatures. A TST calculation predicts the rate constant for the reversible exchange reaction to be $1.06 \times 10^6$ $cm^3$ $mol^{-1}$ $s^{-1}$ at 300 K, in good agreement with experimental data.

**Acknowledgment.** This work was sponsored partially by Emory University and partially by the Caltech Multidisciplinary University Research Initiative under ONR grant no. N00014-95-1388, Program Manager Dr. J. Goldwasser. One of us (X.L.) thanks the Cherry L. Emerson Center for Scientific Computation for financial support.

## References and Notes

(1) Kuo, K. K.; Summerfield, M. *Fundamentals of Solid Propellant Combustion, Progress in Astronautics and Aeronautics*; AIAA: New York, 1984; Vol. 90.

(2) Alexander, M. H.; Dagdigian, P. J.; Jacox, M. E.; Kolb, C. E.; Melius, C. F.; et al. *Prog. Energy Combust. Sci*. **1991**, *17*, 263.

(3) Adams, G. F.; Shaw, R. W., Jr. *Annu. Rev. Phys. Chem.* **1992**, *43*, 311.

(4) Mebel, A. M.; Lin, M. C.; Morokuma, K.; Melius, C. F. *J. Phys. Chem*. **1995**, *99*, 6842.

(5) Diau, E. W. G.; Lin, M. C.; He, Y.; Melius, C. F. *Prog. Energy Combust. Sci*. **1995**, *21*, 1.

(6) Mebel, A. M.; Lin, M. C.; Morokuma, K. *Int. J. Chem. Kinet*. **1998**, *30*, 729.

(7) Mebel, A. M.; Lin, M. C.; Melius, C. F. *J. Phys. Chem*. **1998**, *102*, 1803.

(8) Lu, X.; Park, J.; Lin, M. C. Manuscript in preparation.

(9) Becke, A. D. *J. Chem. Phys*. **1992**, *96*, 2155.

(10) Becke, A. D. *J. Chem. Phys*. **1992**, *97*, 9173.

(11) Becke, A. D. *J. Chem. Phys*. **1993**, *98*, 5648.

(12) Lee, C.; Yang, W.; Parr, R. G. *Phys. Rev*. **1988**, *B37*, 785.

(13) Hehre, W.; Radom, L.; Schleyer, P. v. R.; Pople, J. A. *Ab Initio Molecular Orbital Theory*; Wiley: New York, 1986.

(14) Gonzalez, C.; Schlegel, H. B. *J. Chem. Phys*. **1989**, *90*, 2154.

(15) Pople, J. A.; Head-Gordon, M.; Raghavachari, K. *J. Chem. Phys*. **1987**, *87*, 5768.

(16) (a) Purvis, G. D.; Bartlett, R. J. *J. Chem. Phys*. **1982**, *76*, 1910. (b) Hampel, C.; Peterson, K. A.; Werner, H.-J. *Chem. Phys. Lett.* **1992**, *190*, 1. (c) Knowles, P. J.; Hampel, C.; Werner, H.-J. *J. Chem. Phys*. **1994**, *99*, 5219. (d) Deegan, M. J. O.; Knowles, P. J. *Chem. Phys. Lett.* **1994**, *227*, 321.

(17) Mebel, A. M.; Morokuma, K.; Lin, M. C. *J. Chem. Phys*. **1995**, *103*, 7414.

(18) Curtiss, L. A.; Raghavachari, K.; Trucks, G. W.; Pople, J. A. *J. Chem. Phys*. **1991**, *94*, 7221.

(19) Frisch, M. J.; Trucks, G. W.; Schlegel, H. B.; Gill, P. M. W.; Johnson, B. G.; Robb, M. A.; Cheeseman, J. R.; Keith, T.; Petersson, G. A.; Montgomery, J. A.; Raghavachari, K.; Al-Laham, M. A.; Zakrzewski, V. G.; Ortiz, J. V.; Foresman, J. B.; Cioslowski, J.; Stefanov, B. B.; Nanayakkara, A.; Challacombe, M.; Peng, C. Y.; Ayala, P. Y.; Chen, W.; Wong, M. W.; Andres, J. L.; Replogle, E. S.; Gomperts, R.; Martin, R. L.; Fox, D. J.; Binkley, J. S.; Defrees, D. J.; Baker, J.; Stewart, J. P.; Head-Gordon, M.; Gonzalez, C.; Pople, J. A. *Gaussian 94*, revision D.3; Gaussian, Inc.: Pittsburgh, PA, 1995.

(20) MOLPRO is a package of ab initio programs written by H.-J. Werner and P. J. Knowles, with contributions from J. Almlöf, R. D. Amos, M. J. O. Deegan, S. T. Elbert, C. Hampel, W. Meyer, K. Peterson, R. Pitzer, A. J. Stone, P. R. Taylor, and R. Lindh.

(21) Menoux, V.; Le Doucen, R.; Haeusler, C.; Deroche, J. C. *Can. J. Phys*. **1984**, *62*, 322 and references therein.

(22) McKellar, A. R.; Watson, J. K. G.; Howard, B. J. *Mol. Phys*. **1995**, *86*, 273.

(23) Lee, T. J.; Rice, J. E.; Scuseria, G. E.; Schaefer, H. F., III. *Theor. Chim. Acta* **1989**, *75*, 81.

(24) Duarte, H. A.; Proynov, E.; Salahub, D. R. *J. Chem. Phys*. **1998**, *109*, 26.

(25) Lu, X. Unpublished results.

(26) Laidler, K. J. *Chemical Kinetics*, 3rd ed.; Harper and Row: New York, 1987.

(27) Tokmakov, I. V.; Park, J.; Gheyas, S.; Lin, M. C. *J. Phys. Chem. A*. **1999**, *103*, 3636.

(28) Kaiser, E. W.; Japar, S. M. *J. Phys. Chem*. **1978**, *82*, 2753.

(29) Musin, R. N.; Lin, M. C. *J. Phys. Chem. A* **1998**, *102*, 1808.

(30) Jursic, B. S. *Chem. Phys. Lett*. **1999**, *299*, 334.

(31) Pagsberg, P.; Ratajczak, E.; Sillesen, A.; Latajka, Z. *Chem. Phys. Lett*. **1994**, *227*, 6.